THE JOURNAL OF PHYSICAL CHEMISTRY B

Article

pubs.acs.org/JPCB

Revisiting Point FRAP to Quantitatively Characterize Anomalous Diffusion in Live Cells

Matthew K. Daddysman and Christopher J. Fecko*

Department of Chemistry, University of North Carolina at Chapel Hill, Chapel Hill, North Carolina 27599-3290, United States

Supporting Information

ABSTRACT: Fluorescence recovery after photobleaching (FRAP) is widely used to interrogate diffusion and binding of proteins in live cells. Herein, we apply two-photon excited FRAP with a diffraction limited bleaching and observation volume to study anomalous diffusion of unconjugated green fluorescence protein (GFP) *in vitro* and in cells. Experiments performed on dilute solutions of GFP reveal that reversible fluorophore bleaching can be mistakenly interpreted as anomalous diffusion. We derive a reaction-diffusion FRAP model that includes reversible photobleaching, and demonstrate that it properly accounts for these photophysics. We then apply this model to investigate the diffusion of GFP in HeLa cells and polytene cells of *Drosophila* larval salivary glands. GFP exhibits anomalous diffusion in the cytoplasm of both cell types and in HeLa nuclei. Polytene nuclei contain optically resolvable chromosomes, permitting FRAP experiments that focus separately on chromosomal or interchrosomal regions. We find that GFP exhibits anomalous diffusion in chromosomal regions but diffuses normally in regions devoid of chromatin. This observation indicates that obstructed transport through chromatin and not crowding by macromolecules is a source of anomalous diffusion in polytene nuclei. This behavior is likely true in other cells, so it will be important to account for this type of transport physics and for reversible photobleaching to properly interpret future FRAP experiments on DNA-binding proteins.

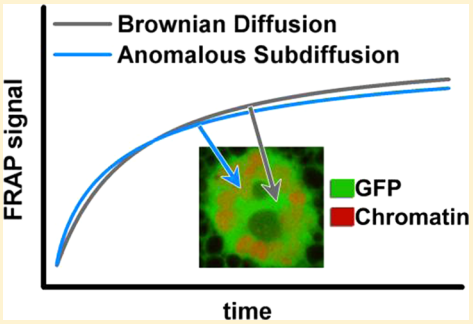

INTRODUCTION

Many biological processes rely on the diffusive transport of proteins in cellular environments that are crowded by a high concentration of macromolecules. Previous studies have established that proteins typically exhibit anomalous subdiffusion under these conditions.[1−8] As opposed to normal Brownian diffusion in which mean squared displacement grows linearly in time, anomalous diffusion is characterized by a mean squared displacement that follows a sublinear power law in time, $\langle \Delta r^2 \rangle \propto t^{\alpha}$. Theoretical studies have indicated that anomalous diffusion may increase the efficiency with which proteins bind to target sites,[9,10] but the physical origin of this behavior is not entirely clear.

Non-Brownian diffusion is predicted by several theoretical models, including mass transport in the presence of a broad distribution of energetic traps (specific and/or nonspecific binding partners), obstructed diffusion in the presence of immobile fractal obstacles, or correlated motion that arises in an interacting system such as a polymer network.[11,12] Anomalous protein diffusion in cells is likely due to a combination of these origins, but it would be useful to devise experiments that probe individual contributions. Previous studies that use noninteracting tracer molecules to eliminate the possibility of binding interactions have observed anomalous diffusion in cells.[5−8] However, it is more difficult to separate the impact of immobile obstacles from the impact of correlations due to macromolecules in a biologically relevant environment. The main purpose of the present study is to isolate contributions from these two physical origins in cell nuclei by separately probing diffusion in regions that contain chromosomes and regions that are devoid of chromatin. Both regions are crowded by a high concentration of mobile macromolecules, but the chromosomal regions additionally contain relatively immobile obstacles (chromatin) that have been suggested to exhibit fractal behavior.[5] We investigate these regions separately by applying fluorescence recovery after photobleaching (FRAP) to diffraction-limited regions of polytene cell nuclei. Polytene nuclei contain giant, optically resolvable chromosomes in interphase, in contrast to more typical cell types in which chromatin is too diffuse to be resolved with conventional optics.

FRAP is used widely in live cell microscopy for assessing the movement and binding of fluorescent molecules. Experiments are typically performed by photobleaching a spatially limited region within a fluorescent sample, and then observing the subsequent evolution of fluorescence from that same region. The time-dependent signal recovery can be related to a molecular process such as diffusion, directed transport, binding interactions, and chemical reactions.[13,14] Early implementations of FRAP used a stationary focused laser beam to quantitatively measure diffusion coefficients of fluorescent species (hereafter referred to as point FRAP), mostly for membrane samples in

Received: October 18, 2012
Revised: December 19, 2012
Published: January 11, 2013

which diffusion is constrained to two dimensions.[15] The development of commercial confocal microscopes led to the widespread application of FRAP methods that bleach spatial regions much larger than the diffraction limit by scanning the focused laser spot within the sample (hereafter referred to as area FRAP).[16−19] Although this latter method is straightforward to implement, the use of arbitrarily shaped bleach regions, three-dimensional diffusion, and sample heterogeneities makes it technically challenging to extract meaningful quantitative information from the experimental data. As a result, many FRAP studies in recent literature are inherently qualitative in nature. Such qualitative measurements are acceptable for some applications, but it is important to recognize their limitations and to adopt a more rigorous approach when necessary. This issue is often not sufficiently considered in studies that attempt to extract microscopic information by fitting area FRAP data according to a kinetic model derived using various simplifying assumptions, some of which may not be appropriate for the experimental conditions,[20] resulting in poor agreement of corresponding parameters reported by various studies. For example, the residence time for one transcription factor reported by two studies differed by about 4 orders of magnitude.[21]

The original implementation of quantitative FRAP was intended to measure the mobility of fluorescence particles in a membrane,[15] so the bleach region of interest is the microscope point spread function projected onto a two-dimensional surface. To apply an analogous point FRAP technique to three-dimensional samples, it is advantageous to restrict the bleach volume in the axial dimension by using two-photon excitation. Nonresonant two-photon absorption is the process by which a molecule exposed to a high photon flux interacts with two photons simultaneously, producing an excited state equivalent in energy to the summation of the energy of the interacting photons.[22] Two-photon microscopy takes advantage of this phenomenon by combining the nonlinear intensity dependence with a steeply decreasing intensity profile outside of the focal point of the objective lens to enhance imaging depth discrimination.[23,24] The diffusion equations have been solved for multiphoton FRAP bleach and observation profiles previously.[25−27] Although point FRAP is not commonly used currently compared to other FRAP methods, we see several advantages for perfecting this method, especially the use of a well-defined bleaching-observation region and sufficiently high time resolution to capture all relevant dynamic processes. The main disadvantage is a decreased signal-to-noise ratio, requiring the collection of numerous data sets to achieve acceptable results. In some cases, point FRAP measurements could be used to complement area FRAP methods and fluorescent correlation spectroscopy (FCS) in order to fully characterize diffusion and binding over a wide range of time scales inside living cells.

This paper investigates the use of two-photon excitation point FRAP to quantitatively assess diffusion of unconjugated enhanced green fluorescent protein (GFP) *in vitro*, in HeLa cells, and in polytene cells of *Drosophila* salivary glands. By using the polytene cells and point FRAP, we are able to separately probe GFP diffusion in the presence (chromatin) and absence (interchromatin space) of relatively immobile DNA obstacles in the nucleus. In addition to extracting diffusion coefficients, we have examined whether a model that includes anomalous diffusion[28,29] is required to fit the FRAP results. The observation and degree of anomalous subdiffusion could provide information about the nature of molecular obstructions or transient interactions, but previous studies have arrived at varying conclusions about the nature of free protein diffusion in cells.[1−8] We find that, in addition to transport physics (diffusion), it is critical to carefully consider the impact of reversible fluorophore bleaching photophysics to accurately interpret time-dependent FRAP recoveries.[30−32] If not taken into account, signal contributions from photophysics can cause normally diffusing fluorophores to appear to exhibit anomalous diffusion. When these photophysics are properly modeled, GFP diffusion in the solution samples is normal but most of the cellular regions exhibit some degree of anomalous diffusion. One notable exception to this trend is the interchromatin space of polytene nuclei, in which GFP exhibits normal diffusion.

MATERIALS AND METHODS

1. Sample Preparation. Purified enhanced green fluorescent protein was a generous gift from Dr. Gary Pielak. The GFP was diluted to a concentration of 10 μM in phosphate buffered saline (PBS) for the aqueous solution measurements. For samples in glycerol, GFP was diluted in a solution of 62% (w/w) glycerol (n_D = 1.4151 at 20 °C)[33] to a final concentration of 10 μM GFP and 60% glycerol. Alexa Fluor 488 (Invitrogen, Carlsbad, CA) was diluted to a final concentration of 10 μM in PBS. Polyacrylamide GFP gels were made by diluting the GFP stock to a concentration of 10 μM in a 1:1 mixture of 40% acrylamide (Fisher Scientific, Fair Lawn, NJ) and 2% bisacrylamide (Fisher Scientific). To form the gel, 1 μL of tetramethylethylenediamine (Fisher Scientific) and 1 μL of ammonium persulfate (Fisher Scientific) were added to 200 μL of the acrylamide GFP mixture. The mixture was then quickly transferred to a glass bottom culture dish (MatTek Corporation, Ashland, MA) and sealed with another coverslip. The gel was allowed to polymerize for 1 h before the experiment.

HeLa cells stably expressing GFP (Cell Biolabs, Inc., San Diego, CA) were cultured in phenol-red free Dulbecco's modified Eagle's medium (Gibco, Billings, MT) supplemented with antibiotics and 10% fetal bovine serum (Gibco) at 37 °C and 5% CO_2. For FRAP experiments, cells were seeded on MatTek glass bottom culture dishes at a density of 2.5 × 10^5 cells per dish ∼18 h before the experiment.

Polytene cells were imaged in intact salivary glands extracted from transgenic *Drosophila melanogaster* larvae. The larvae were produced by crossing a transgenic fly line that expresses free GFP with another transgenic line that expresses a histone 2B (H2B)-mRFP fusion protein. The fluorescent histones were used to permit the differentiation of chromosomal and nucleoplasmic regions using two-color imaging. The transgenic line that expresses the H2B-mRFP fusion protein under the control of a Gal4 upstream activation sequence was described in Zobeck et al.;[34] the protein was expressed in salivary gland cells by generating a homozygous cross with the c147 *Gal4* driver line (Bloomington Stock Center line #6979). This homozygous cross was mated with the line containing a GFP transgene (Bloomington Stock Center line #5430), which was also under the control of a *Gal4* upstream activating sequence. Larva were raised at room temperature in standard cornmeal yeast medium, collected at the third-instar stage 8−9 days after eggs were laid, and dissected in Grace's Insect Medium (Gibco). For FRAP experiments, salivary glands were transferred to a MatTek glass-bottomed culture dish in Grace's medium and gently sealed under another glass coverslip to

minimize sample movement. All experiments were completed within 1 h after salivary gland extraction.

2. Two-Photon Microscope Setup. FRAP experiments were performed with a home-built laser-scanning two-photon microscope.[35] A near-infrared Coherent Chameleon Ultra II Ti:sapphire oscillator produced femtosecond pulses at a wavelength maximum of 950 nm and a repetition rate of 80 MHz. An electro-optic modulator with a 1 μs response time (Conoptics 350-80LA/BK) and polarizer placed directly after the laser controlled the intensity used for imaging and FRAP. Note that any mention of the laser power in the procedures actually refers to the power transmitted by the electro-optic modulator and measured at the objective (e.g., turning the laser off means that the power transmitted by the modulator was extinguished). Galvanometer-mounted mirrors and relay lenses in the beam path determined the angle with which the laser beam enters a 60×, 1.2 NA water-immersion objective lens mounted on an Olympus IX81 inverted microscope. Computer control of this incident angle is used to raster scan images of the sample or point the beam for point FRAP experiments. The back aperture of the lens was slightly overfilled to maintain a tight focus; the point spread function was determined by imaging 100 nm diameter immobilized fluorescent microspheres (ω_r = 293 nm and ω_z = 951 nm). The imaging and FRAP bleach and observation powers were measured after the objective using a calibrated power meter. Epifluorescence was detected by a Hamamatsu H7422P-40MOD nondescanned GaAsP photomultiplier tube (PMT) module. To detect GFP fluorescence, a 510/70 bandpass filter was placed in front of the PMT. For multicolor experiments, the epifluorescence beam was split using a 570 dichroic mirror to a GaAs PMT (Hamamatsu H7422P-50MOD) with a 630/100 bandpass filter for detecting mRFP fluorescence. Signals from the PMTs were processed and enhanced by high gain preamplifiers. The output from the preamplifiers was read into an A/D card (National Instruments) with a sampling time of 100 ns; 10 samples were averaged to produce 1 μs time points during data collection. We note that the high gain preamplifers we typically use for imaging dim samples could not recover quickly enough from the voltage saturation that occurred during the bleach pulse. The reduced gain, a result of saturation, recovered on the time scale of several milliseconds, obscuring the bleach recovery. This "detector blinding" effect and the methods used to characterize it have been reported previously.[21] One possible method of correcting for the detector blinding effect was to reduce the gain on the PMT during the bleach pulse, but the gain control on the PMT electronics was too slow. Therefore, we used a modified current preamplifier (sensitivity of 20 μA/V), which was designed to minimize the impact of signal saturation during bleaching.

3. FRAP Procedure. To identify regions of interests, an image was acquired using Labview-based software developed in-house and then one or more points were selected for bleaching. In cellular samples, care was taken to ensure selected points were sufficiently far from membranes. FRAP data were collected at each point using an intermittent data collection scheme designed to reduce observational photobleaching by only illuminating the sample for a small fraction of the time it takes the fluorescence to fully recover from a 20 μs bleach. Details of this scheme are provided in Figure 1 and in the Supporting Information. Control data sets were taken with the same timing sequence at the observation power except with a 20 μs mock bleach (i.e., the observation power is used in place

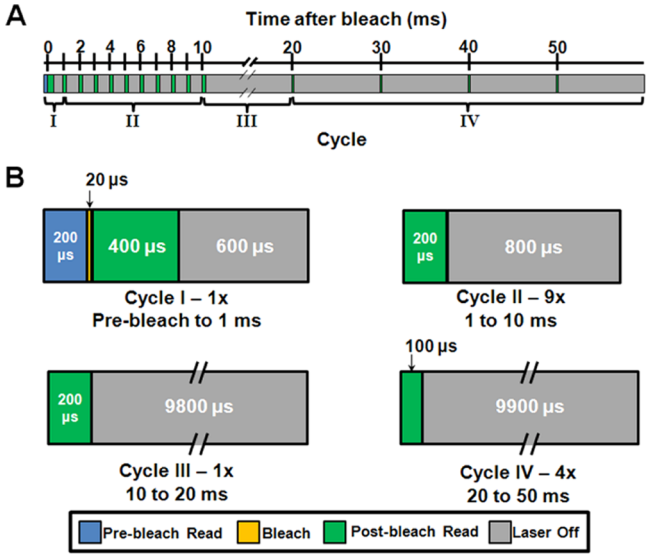

Figure 1. Timing diagram of the point FRAP method. (A) One FRAP measurement covered 50 ms, which was broken up into four different cycles as described in panel B. (B) Timing within each cycle is shown in detail. The number of times that each cycle was repeated is indicated by the number of repeats followed by an ×; e.g., cycle II was repeated 9 times indicated by 9×. Prebleach and postbleach reads indicate that the observation laser power was applied and data collected, bleach indicates that the bleaching laser power was applied, and laser off indicates that the laser power was extinguished during that period.

of the bleach power). Five hundred replicates were taken for both the bleach and control curves to improve the signal-to-noise ratio, which obeyed Poisson statistics (Figure S1, Supporting Information). Each replicate was normalized to the average of the prebleach values before averaging replicates. In all figures except Figure 3, FRAP data are obtained by dividing the bleach data set by the control data set. All measurements were made at room temperature (22 °C).

4. Fitting and Statistical Model. FRAP data was fit to the curve in eq 4 or 6 using the *lsqnonlin* routine in MATLAB (The MathWorks, Natick, MA). Data collected during the first 50–70 μs following the bleach were excluded from the fits to eliminate the influence of detector/preamplifier saturation (Figure S2, Supporting Information). The fitting equations included a floated parameter to measure an immobile fraction; however, we found that the value was always within the noise of the measurement, indicating no immobile fraction. The residuals were weighted to emphasize early time points in the FRAP recovery and to account for the gaps in data collection. To account for a broad range of recovery time scales, FCS data is binned logarithmically in time. In analogy, we weighted residuals of data points spaced equally in time by the inverse of the time after bleaching, which is mathematically equivalent to spacing the points logarithmically. Details on fitting are provided in the Supporting Information.

When fitting for anomalous diffusion, an additional parameter (an anomalous exponent) was introduced into the model; as a result, fits using the anomalous diffusion model usually had lower residuals than normal diffusion. However, this lower residual does not necessarily justify the additional degree of freedom introduced into the fitting model. To statically distinguish the better of the two candidate models, we applied the Bayesian information criterion (BIC).[36−38] The advantage

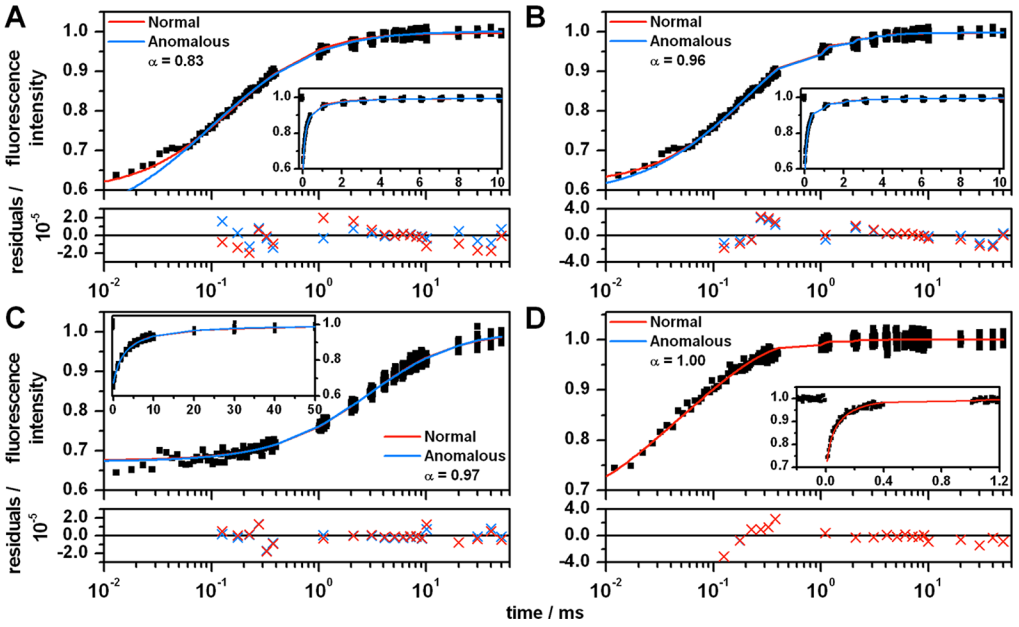

Figure 2. *In vitro* point FRAP data (points) and fits (lines) plotted using logarithmic time axes and linear time axes (inset). For clarity, the fit residuals (lower plot in each panel) were averaged over 50 μs intervals from 100 to 400 μs (cycle I) and for each read time period of either 100 or 200 μs (cycles II–IV). (A) GFP in a PBS solution fit by a FRAP model that does not account for reversible bleaching. The data were fit to eq 4 using a value of α that was either fixed to 1.0 (normal diffusion) or floated in the fit (anomalous diffusion). For the normal diffusion fit, D is equal to 76 ± 2 $\mu m^2\ s^{-1}$, and for the anomalous diffusion fit, D_{eff} is equal to 100 ± 17 $\mu m^2\ s^{-1}$. (B–D) FRAP data fit by a model that accounts for reversible bleaching (eq 6). Again, the value of α was either fixed to 1.0 (normal diffusion) or floated in the fit (anomalous diffusion). The samples are GFP in PBS (B), GFP in 60% glycerol (C), and Alexa Flour 488 in PBS (D).

of this test over other similar statistical tests was that for large sample sizes ($n \approx 2700$) the BIC still penalizes for extra parameters. The BIC value for each model, i, was calculated by

$$\mathrm{BIC}_i = n \ln\left(\frac{\mathrm{res}_i}{n}\right) + K_i \ln(n) \quad (1)$$

where n was the number of data points fit, res_i was the square root of the sum of the squares of the residuals of the fit for each model i, and K_i was the number of parameters for each model ($K = 4$ for normal diffusion and $K = 5$ for anomalous diffusion). The candidate with the lowest BIC score was considered to be the better model. To quantify the likelihood that each candidate represents the true model, we used

$$\Delta_i = \mathrm{BIC}_i - \min \mathrm{BIC} \quad (2)$$

to calculate the Akaike weight, w_i, of each model according to

$$w_i = \frac{\exp(-0.5\Delta_i)}{\sum_{j=1}^{J} \exp(-0.5\Delta_j)} \quad (3)$$

where J is the total number of candidate models ($J = 2$). These Akaike weights are the probability that each candidate is the true model.

RESULTS

1. GFP Appears to Exhibit Anomalous Subdiffusion in Solution. Particles that diffuse freely in simple systems typically exhibit normal Brownian diffusion, which is characterized by a mean square displacement that grows linearly with time $\langle \Delta r^2 \rangle = 2dDt$, where d is the dimensionality of the system and D is the diffusion coefficient. In more complex systems, particles may exhibit anomalous diffusion in which the mean squared displacement follows a nonlinear power law in time $\langle \Delta r^2 \rangle = 2d(\Gamma/\alpha)t^\alpha$, where Γ is the transport coefficient and α is the anomalous exponent. (We note that previous literature contains several different definitions for the transport coefficient and that we have adopted the approach proposed by Kang et al.[39]) The signal measured in a two-photon excited point FRAP experiment derived by Brown et al.[25] and modified to include anomalous diffusion is

$$F(t) = F_0 \sum_{n=0}^{\infty} \frac{(-\beta)^n}{n!} \left[1 + n\left(1 + \frac{16\Gamma t^\alpha}{\alpha \omega_r^{\,2}}\right)\right]^{-1} \left[1 + n\left(1 + \frac{16\Gamma t^\alpha}{\alpha \omega_z^{\,2}}\right)\right]^{-1/2} \quad (4)$$

where F_0 is the prebleach fluorescence intensity, β is a factor related to the bleach depth, and ω_r and ω_z are the size of the focused Gaussian beam in the radial and axial dimensions, respectively.

We initially used this eq 4 to estimate the time range necessary to experimentally characterize diffusion in vitro and in cells. Assuming normal diffusion with a diffusion coefficient typical for unconjugated GFP in solution (80 $\mu m^2\ s^{-1}$),[31] a moderate bleach depth, and the size of our focused laser, the fluorescence signal recovers halfway from its bleached value in about 140 μs and 90% from its bleached value in about 1 ms. Using subdiffusive values in the range that has been reported for GFP in cells ($\alpha \sim 0.8$, $\Gamma \sim 20$ $\mu m^2\ s^{-1}$), the half and 90% recovery values are about 2 and 25 ms, respectively. We cover this range of experimental time scales using a detection system with microsecond observation time bins collected over a period of 50 ms after the initial bleach. To avoid excessive photobleaching (and photophysical processes discussed below), we adopt an intermittent data collection strategy that

dx.doi.org/10.1021/jp310348s | J. Phys. Chem. B 2013, 117, 1241–1251

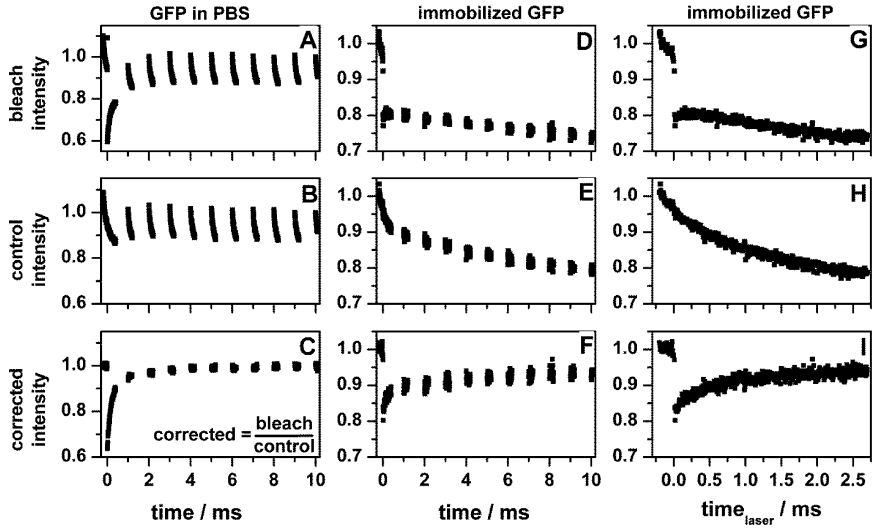

Figure 3. Demonstration of the importance of accounting for reversible fluorophore bleaching. (A–C) Raw FRAP signals of GFP in PBS, including the bleach (A) and control (B) data before division. Note that all other figures plot only the corrected (bleach divided by control) FRAP data (C). The necessity of this division is demonstrated by the rapid photobleaching of new fluorophores that have diffused into the observation volume during the laser off times; the division removes this rapid photobleaching, as demonstrated by the long time points. (D–F) Raw FRAP signals of GFP immobilized in a polyacrylamide gel. The corrected (F) curve showed a recovery even though diffusion was not present. The source of this apparent recovery was that the slope of the control curve (E) was steeper than the bleach curve (D) due to the non-exponential nature of the bleaching photophysics. (G–I) The same data from parts D–F was plotted on a laser time axis showing only the laser on time and removing the laser off time gaps. Note that the data are continuous, demonstrating that the time-dependent signals are light driven and that the recovery is not due to incomplete immobilization. Also, the fluorescence recovery during the laser off time is negligible. Therefore, the reversible photobleaching correction depends only on the laser illumination time, t_{laser}, rather than the actual time after photobleaching.

involves toggling the observation laser power on and off during the 50 ms period (Figure 1). In analogy with fluorescence correlation spectroscopy (FCS), the broad time range over which the FRAP signal recovers lends itself to data binned logarithmically in time. Rather than directly collecting data spaced in this way, we fit data collected according to the aforementioned sequence using a weighting algorithm equivalent to logarithmically binning data points (see the Supporting Information). The analogy with FCS also prompted us to plot data using logarithmic time axes, which is beneficial for visualizing signals that vary over a large range of time.

To verify that our data collection and analysis method correctly determines diffusion coefficients, we measured the diffusion coefficient of GFP in PBS (Figure 2A). We fit point bleach curves to eq 4 using either a value of α that was fixed to 1.0 (normal diffusion) or floated in the fit (anomalous diffusion). We were surprised to find that the FRAP curves were best fit by the anomalous diffusion model with exponents (α) as low as 0.8. (According to a BIC statistical analysis, the anomalous diffusion model was nearly always more likely than normal diffusion, sometimes with 100% likelihood.) This result is clearly not consistent with simple Brownian diffusion. In contrast, FRAP curves of GFP in 60% glycerol consistently exhibited recoveries that were nearly Brownian.

While the observation of anomalous diffusion in dilute solution could have been attributed to various experimental inaccuracies, one set of additional experiments revealed that the model used to fit the data was the source of the problem. To obtain the GFP FRAP data, we had corrected for observational photobleaching using a standard method, by dividing the fluorescence signal from a sample that had been intentionally bleached by the signal from a control sample that had not been intentionally bleached (Figure 3A–C). However, this correction may not fully account for the photophysics observed in the data. Mueller et al.[20] reported an unexpected signal contribution in some FRAP experiments that arises from reversible photobleaching. To determine the influence of these photophysics on our data, we fixed GFP in a polyacrylamide gel and conducted FRAP experiments (Figure 3D–F). By fixing the sample and thus eliminating the transport physics from consideration, signal contributions from reversible fluorophore photophyiscs are exposed. Even though the raw bleach curve (Figure 3D) does not exhibit a recovery and in fact shows slow photobleaching, the corrected curve (Figure 3F) clearly exhibits a recovery. This apparent recovery arises from a decay of the control curve (Figure 3E) at early times that is absent from the bleach curve. This observation led us to question the validity of correcting for observational photobleaching by dividing the bleach curve by a control curve, a practice common to nearly all FRAP methods. The fundamental assumption behind this procedure is that the photobleaching kinetics at a particular observation power are independent of initial conditions. Although true for a first-order process, this condition is not satisfied in the case of highly non-exponential bleaching kinetics. Thus, a model that accounts for more realistic bleaching photophysics is required.

2. FRAP Model That Accounts for Reversible Photobleaching. Single-molecule spectroscopy has established that one primary source of non-exponential photobleaching kinetics is the intermittency (i.e., "blinking") exhibited by nearly all fluorophores.[40] This universal behavior can be incorporated by considering a photophysical model in which fluorophores (Fl) can be converted to either a reversibly bleached (RB) or an irreversibly bleached (IB) state:[41]

$$\mathrm{RB} \underset{k_{-1}}{\overset{k_1}{\rightleftharpoons}} \mathrm{Fl} \overset{k_2}{\rightarrow} \mathrm{IB} \qquad (5)$$

dx.doi.org/10.1021/jp310348s | J. Phys. Chem. B 2013, 117, 1241–1251

The conceptual and mathematical impact of this photophysical process on a FRAP measurement is provided in the Supporting Information. In brief, irradiation of a sample disturbs the pre-existing equilibrium of Fl and RB states, leading to a relaxation process that approaches a new equilibrium value with a rate constant given by the sum of the forward and reverse reactions. Because these photochemical transformations depend on the intensity of light, the bleached sample approaches the new equilibrium much more rapidly (likely during the bleach pulse) than the control sample. Thus, the control curve contains a decay at short times whose amplitude is absent (or greatly reduced) in the bleach curve. Both curves decay similarly at longer times due to irreversible fluorophore bleaching. Therefore, dividing the bleach curve by the control curve correctly accounts for irreversible bleaching but also introduces a signal contribution due to reversible bleaching. The contributions of these processes to a FRAP signal are complicated by diffusion, but our reaction-diffusion model includes coupled equations that account for both transport physics and photophysics.

In the presence of reversible photobleaching, the FRAP signal (derived in the Supporting Information) is

$$F(t) = F_0\left[1 + \delta \exp\left(\frac{-t_{\text{laser}}}{\tau_{\text{PP}}}\right)\right] \sum_{n=0}^{\infty} \frac{(-\beta)^n}{n!}\left[1 + n\left(1 + \frac{16\Gamma t^{\alpha}}{\alpha\omega_r^{\,2}}\right)\right]^{-1}\left[1 + n\left(1 + \frac{16\Gamma t^{\alpha}}{\alpha\omega_z^{\,2}}\right)\right]^{-1/2} \quad (6)$$

In comparison to eq 4, reversible bleaching introduces an additional factor that depends on the photophysics decay time constant, τ_{PP}, and magnitude, δ. This factor depends on t_{laser}, which is the time that the laser has irradiated the sample; it differs from the time dependence of the diffusion factors because we applied an intermittent data collection scheme. The dependence on t_{laser} is motivated by the observation that the photophysical signal varies only when the laser is on, as demonstrated by the lack of signal change during laser off times in immobilized samples (Figure 3G–I). This observation is consistent with transformations driven by photon absorption.

To examine the influence of the photophysical correction on the FRAP signal, normal (Brownian) diffusion curves with a diffusion coefficient of 82 or 25 $\mu m^2\ s^{-1}$ were simulated using different values of τ_{PP} and δ. The curves were then fit to an anomalous model without a photophysics correction (eq 4). Depending on the exact values of the photoswitching parameters, the diffusion could appear to be normal, subdiffusive, or superdiffusive (Figure 4).

The most straightforward way to fit experimental data according to eq 6 would be to simply float the additional parameters introduced in the photophysical model, τ_{PP} and δ. However, this approach introduces too many degrees of freedom into the model, making it challenging to separate photophysical contributions from anomalous diffusion. One way to isolate the photophysical parameters is to immobilize the GFP and then fit the resulting FRAP curve to the model with a vanishingly small diffusion coefficient. However, we found that δ is very dependent on the bleach depth and small variations in experimental conditions lead to difficulties matching the bleach depth of mobile and immobile samples. After exploring these options, we found that the most reliable procedure to determine the value of δ is to fit the early part of the control curve (for 600 μs) with an exponential to account for reversible bleaching equilibration. This fit gave a similar value of τ_{PP} as the fixed sample and yielded a more accurate δ value for each sample. Therefore, this procedure was used to obtain the values of τ_{PP} and δ, which were then fixed when fitting the corrected FRAP curve according to eq 6.

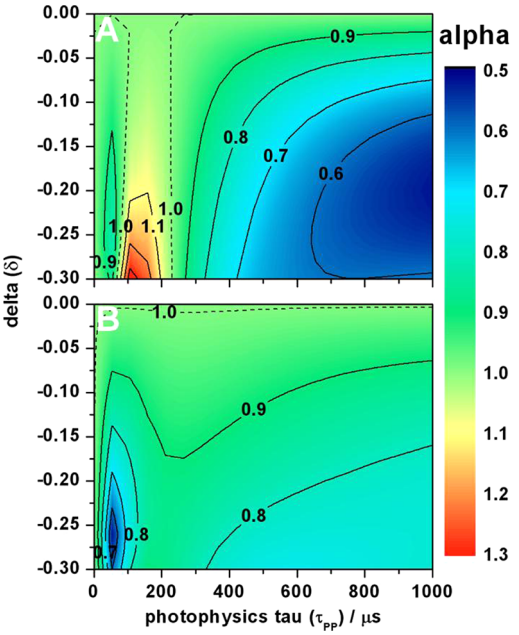

Figure 4. When not taken into account, reversible photobleaching can cause fluorophores that diffuse normally to appear to exhibit anomalous diffusion. Shown are contour plots of the anomalous factor obtained when data simulated by a Brownian diffusion ($\alpha = 1$) FRAP model that includes reversible photobleaching (eq 6) were fit using the FRAP model that did not account for these photophysics (eq 4). Delta and photophysics tau refer to the parameters δ and τ_{PP} in eq 6. The data were simulated using diffusion coefficients of $D = 82\ \mu m^2\ s^{-1}$ (A) or $D = 25\ \mu m^2\ s^{-1}$ (B), the approximate diffusion coefficients of GFP in solution and cellular samples, respectively.

3. Reversible Photobleaching FRAP Model Indicates GFP in Solution Diffuses Normally. After applying the above correction, the anomalous diffusion factor of GFP in PBS changes from 0.83 to 0.96 which is in the same range as the glycerol fits (Figure 2B). More importantly, the BIC value indicated that the normal diffusion model became the more likely of the two after the photophysics correction (Table 1). The diffusion coefficient of GFP was found to be $84 \pm 6\ \mu m^2\ s^{-1}$ in excellent agreement with other sources.[31,42] The glycerol fits (Figure 2C) did not change with the photophysics

Table 1. Summary of Model Fits for GFP in Solution

sample	photophysics correction	type of diffusion	anomalous factor	BIC w_i
GFP in PBS	no	normal	1.00	0.0000
		anomalous	0.82	1.0000
	yes	normal	1.00	0.8806
		anomalous	0.99	0.1194
GFP in 60% glycerol	N/A[a]	normal	1.00	0.1191
		anomalous	0.96	0.8809

[a]Applying the photophysics correction did not change the fits for the glycerol sample.

dx.doi.org/10.1021/jp310348s | J. Phys. Chem. B 2013, 117, 1241–1251

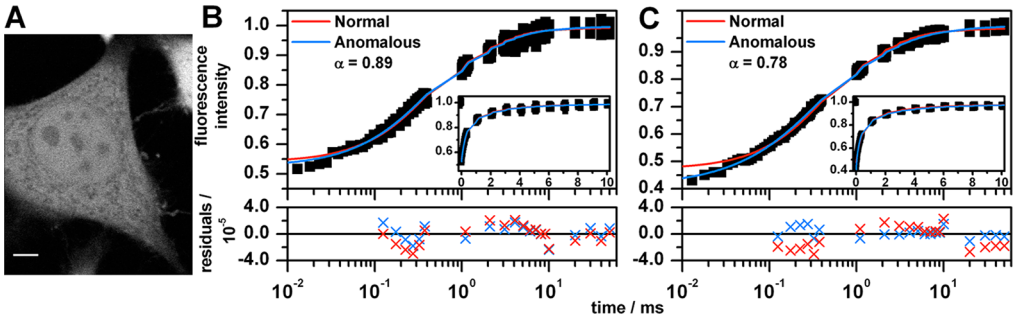

Figure 5. (A) Two-photon microscopy image of a HeLa cell expressing unconjugated GFP. Scale bar, 5 μm. (B–C) FRAP data (points) and fits (lines) of GFP in HeLa cells plotted on logarithmic time axes and linear time axes (inset). The residuals were averaged as in Figure 2. The data were fit to eq 6 using a value of α that was either fixed to 1.0 (normal diffusion) or floated in the fit (anomalous diffusion). The data were recorded by focusing on points in the nucleus (B) and in the cytoplasm (C).

Table 2. Summary of Best Fit Models for GFP and Alexa Flour 488[a]

sample	BIC indicated best model	range of BIC w_i for best model	D (μm^2 s^{-1}) or Γ (μm^2 s$^{-\alpha}$)	α
GFP in PBS	normal	0.8806[b]–0.9797	84 ± 6	
GFP in 60% glycerol	anomalous	0.8809–0.9973	6.2 ± 0.9	0.95 ± 0.01
Alexa Fluor 488 in PBS	normal	0.9637[b]–0.9811	438 ± 12	
GFP in HeLa—nucleus	anomalous	1.0000–1.0000	70 ± 27	0.84 ± 0.05
GFP in HeLa—cytoplasm	anomalous	1.0000–1.0000	130 ± 60	0.76 ± 0.07
GFP in polytene—chromosome	anomalous	1.0000–1.0000	66 ± 1	0.79 ± 0.01
GFP in polytene—interchromatin space	normal	0.9808–0.9809	32 ± 6	
GFP in polytene—cytoplasm	anomalous	1.0000–1.0000	335 ± 236	0.56 ± 0.11

[a]The errors reported are the standard deviation between fits to three independent experiments. [b]One replicate for both PBS and Alexa Fluor 488 had a score of 0.0000 for the normal diffusion model. These models are excluded from the weighting range but are included in the average. The alpha values for both of these models were greater than 0.9.

correction. There are two possible explanations. One is that polyethylene glycol has been shown to have photoprotectant properties,[43] and it is possible that glycerol as the monomer would reduce the impact of photophysics as well. We did observe that our fits to the control curve in the glycerol samples had much larger τ_{PP} than the other samples because the control curve was nearly flat over the time scale of our experiment, indicating that the photophysics correction may not be necessary. The other possible explanation is that the diffusion coefficients measured in glycerol are much slower than any of the other diffusion coefficients measured in this study, perhaps minimizing the impact of rapid photophysics. The 60% glycerol solution shows a 20-fold reduction in the diffusion coefficient which is larger than expected from the 10-fold increase in viscosity over aqueous solution.[44] One possible explanation for this discrepancy is the distortion of the point spread function by glycerol.[45] We were also able to measure the diffusion coefficient of Alexa Fluor 488 in solution (Figure 2D). We found a diffusion coefficient of 438 ± 12 μm^2 s^{-1} in excellent agreement with literature values.[42]

4. GFP Exhibits Anomalous Diffusion in Most Cellular Environments. For all of the unconjugated GFP in cell samples, the FRAP curves were fit with both the normal and anomalous model with the photophysics correction in eq 6. First, HeLa cells expressing unconjugated GFP were imaged (Figure 5A), and FRAP was performed on points in the nucleus and cytoplasm. Diffusion of GFP in both the nucleus (Figure 5B) and cytoplasm (Figure 5C) of HeLa cells was found to be best fit by the anomalous model as indicated by the BIC test, even after accounting for reversible bleaching photophysics (Table 2). The cytoplasm had a smaller anomalous exponent (α = 0.76) than the nucleus (α = 0.84).

Drosophila polytene cells were used because the large cell nuclei contained optically resolvable chromosomes in interphase, in contrast with HeLa cells. Therefore, we could probe the difference between GFP diffusion in nuclear areas that contained chromosomes and in the interchromatin space. To experimentally distinguish between the chromosomal and interchromatin space, the flies coexpressed a histone 2B-mRFP construct that marked chromosomal regions (Figure 6A–C). The GFP was partially excluded from the chromosomes which further helped discriminate between the two regions. GFP diffusion in the chromosome region in the polytene nuclei (Figure 6D) behaved similarly to the HeLa nucleus with an average anomalous factor of 0.79 (Table 2) comparable to the 0.84 value in the HeLa nucleus. In contrast, GFP in the interchromatin space of the polytene nuclei diffuses normally (Figure 7C), though its effective viscosity is 2.6 times that of water (comparable to a 30–40% glycerol solution) which clearly indicates that crowding is occurring (since the base solvent of the cell is also water); however, the crowding does not cause anomalous diffusion. The observation that GFP diffuses normally in the interchromatin space but anomalously within the polytene chromosomes is notable, since neighboring biological regions unseparated by a membrane typically do not exhibit different types (anomalous vs normal) of diffusion. Unconjugated GFP should not interact specifically with DNA or other elements of chromatin, so it is likely that the anomalous diffusion in the chromosomal regions is due to the presence of obstructions. This issue is considered further in the Discussion section. We also investigated GFP diffusion in the cytoplasm of polytene cells (Figure S5, Supporting Information); it exhibited diffusion that was more anomalous than the nucleus, in agreement with the HeLa result.

dx.doi.org/10.1021/jp310348s | J. Phys. Chem. B 2013, 117, 1241–1251

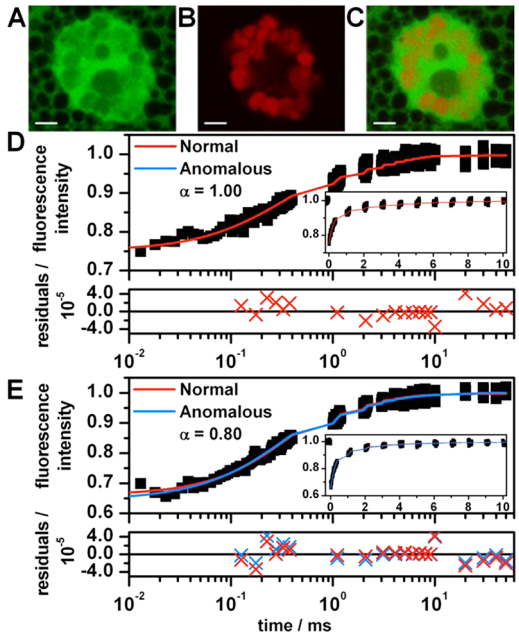

Figure 6. (A–C) Two-photon microscopy images of a polytene cell expressing both unconjugated GFP (A) and H2B-mRFP (B) to mark the chromosomes. Panel C is the merge of panels A and B. Scale bar, 5 μm. (D, E) FRAP data (points) and fits (lines) of GFP in polytene cells plotted on logarithmic time axes and linear time axes (inset). The residuals were averaged as in Figure 2. The data were fit to eq 6 using a value of α that was either fixed to 1.0 (normal diffusion) or floated in the fit (anomalous diffusion). The data were recorded by focusing on points in the interchromatin space (D) and on the chromosomes (E).

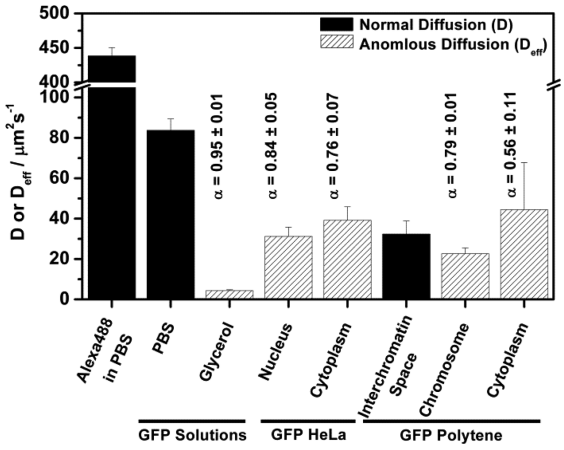

Figure 7. Summary of diffusion (or effective diffusion) coefficients for each sample. Brownian (or normal) diffusion is indicated by the solid bars, and anomalous diffusion is indicated by the striped bars. For anomalous diffusion samples, the effective diffusion coefficients were calculated using dimensions of the focused point spread function, and the average anomalous parameter is listed above the bar. All values are the average of three independent fits of data sets consisting of an average of 500 samples each. The errors are the standard deviation of the fit results.

In order to compare diffusion across samples with different anomalous factors we calculated an effective diffusion coefficient defined as D_{eff}:

$$D_{\text{eff}} \equiv \frac{\omega^2}{6\tau_D} = \frac{\omega^2}{6}\left[\frac{\alpha\omega^2}{6\Gamma}\right]^{-1/\alpha} \quad (7)$$

where τ_D is the residence time (as defined by Kang et al.[39]) for a region of interest of radius ω. The effective diffusion coefficient reflects the diffusion coefficient that would have been measured in the experiment if diffusion were Brownian; its value is specific to the size of the observation region. The transport coefficients and anomalous factors listed in Table 2 (along with the focused spot size) were used to calculate D_{eff}. These values are plotted along with normal diffusion coefficients of samples that exhibited Brownian diffusion in Figure 7. The effective diffusion coefficients of all of the cellular samples were similar regardless of the environment, even though they differed in the magnitude of the anomalous factor.

DISCUSSION

1. Revisiting Point FRAP. We have investigated the use of point FRAP with a diffraction-limited bleach and observation volume to quantitatively characterize fluorophore diffusion. In addition to providing a well-defined region of interest, point FRAP allows for highly specific regions of a cell to be selected, which reduces possible sample heterogeneities within the region of interest. Area FRAP methods with larger observation regions average out these variations. Point FRAP can determine diffusion coefficients over a wide range of time scales due to its superior time resolution over other FRAP methods. When using other FRAP regions of interest, it is necessary to scan over the region of interest which can take tens to hundreds of milliseconds. With point FRAP, we are able to measure diffusion coefficients ranging from 438 $\mu m^2\ s^{-1}$ (Alexa Flour 488) to 4 $\mu m^2\ s^{-1}$ (GFP in glycerol), a range that covers over 2 orders of magnitude. It is quite possible to measure diffusion coefficients that are slower than the one measured for glycerol, as it is straightforward to increase the amount of time that data is collected. Additionally, point FRAP could be used to measure binding on longer time scales. Since binding dynamics can occur over a broad range of time scales, it may be helpful to augment point FRAP measurements with quantitative area FRAP, since this latter method is able to achieve long observation times with less averaging.

FCS can also be used to measure protein dynamics in a diffraction limited spot, but we believe point FRAP offers two advantages over FCS. First, FCS requires a very low concentration (nanomolar) of fluorescent species, which is not always achievable in cellular samples. Point FRAP can be used at a wider range of concentrations and is ideal for samples in which the fluorescent species is highly expressed. Second, in order to measure dynamics, FCS requires constant illumination for seconds or longer, resulting in photobleaching and photodamage artifacts for samples in which there is slow diffusion or an immobile fraction. In point FRAP, the laser may be turned off for periods of time to reduce photobleaching, while the dynamics can still be measured.

2. Application of the Photophysics Correction to General FRAP Procedures. We have demonstrated that it is critical to account for reversible fluorophore photobleaching to extract quantitative information from point FRAP measurements. By separately considering the raw bleach recovery data and control data of an immobilized fluorophore sample, we determined that reversible bleaching primarily affected the control data. This is not a general result; reversible bleaching may affect the raw bleach recovery in other FRAP implementations (including area FRAP, as discussed below). Therefore, we recommend that all FRAP investigations should test for the importance of reversible bleaching by performing

control experiments similar to those in the present study. First, an experiment should be performed where diffusion is eliminated (e.g., by fixation) to isolate the influence of photophysics. If the sample shows recovery, then reversible photobleaching needs to be taken into account, and the raw bleach and control curves of these samples should be carefully investigated separately to determine from what behavior photophysics anomaly is arising. Another test is to measure the recovery in solution to ensure that the sample recovers according to Brownian diffusion, though of course this test only applies to FRAP implements with sufficient time resolution to observe diffusion.

The FRAP model we have derived (eq 6) can generally account for the influence of reversible bleaching in the raw bleach curve and/or in the control curve. However, because only the control curve was affected by reversible bleaching in our experiments, we chose to implement the model in a way that specifically accounts for this case. Determining the reversible bleach parameters by fitting the initial decay of the control curve would not yield accurate results if the raw bleach curve were also influenced by reversible bleaching.

We also note that the importance of accounting for reversible photobleaching is not specific to point FRAP experiments. This assertion is substantiated by a recent study in which McNally and co-workers[32] demonstrated the detrimental impact of reversible photoswitching on area FRAP experiments of nuclear proteins. Given the ~600 μs photophysics time scale measured in the present study, it may sound surprising that area FRAP measurements on much longer time scales (time resolution of milliseconds to seconds) would be affected by reversible bleaching. However, the time scale for photobleaching reversion is affected by illumination intensity;[41] reversion takes much longer at lower light intensities and can even proceed in the absence of illumination with time constants of a few seconds. Thus, FRAP experiments on much longer time scales can be affected by reversion. Additionally, area FRAP experiments that employ high intensity focused illumination can be affected by reversion on long time scales because each pixel is typically only illuminated for a few microseconds per frame. Raster scanning the focused laser effectively introduces an intermittent illumination, similar to the intermittent scheme employed in the present point FRAP experiments; the cumulative experimental time after photobleaching does not accurately reflect the time that each pixel has actually been irradiated. In conclusion, it is difficult to generally assess the importance of reversible photobleaching on various FRAP procedures, so it is important to test for the importance of reversible bleaching as discussed above.

3. Observation of Both Normal and Anomalous Diffusion in Live Cells. The detection of anomalous diffusion in most of the cellular samples is consistent with several previous findings.[5−8] However, the observation of Brownian diffusion in the interchromatin space of polytene nuclei is unique. Unlike normal diploid cells where the chromatin is diffuse and occupies the entire nucleus, polytene cells contain large chromosomes between which are regions of nucleoplasm that is free of DNA. Our point FRAP measurements indicate that unconjugated GFP diffuses normally in these interchromatin spaces, while it exhibits anomalous diffusion in the chromosomal regions of the same cell. This result is notable for several reasons. First, since anomalous diffusion is observed only in chromosomal regions of the polytene cells, it is likely that the primary crowding agent responsible for anomalous diffusion in the nucleus of other cell types is chromatin. Although this result is not entirely surprising, it has been suggested that the high degree of macromolecular crowding in cells could generally cause anomalous diffusion. The interchromatin space exhibits a viscosity about 2.6 times that of water and it undoubtedly contains high concentrations of macromolecules other than DNA, yet GFP diffuses freely. We therefore conclude that transport through chromatin, and not crowding by other macromolecules, causes unconjugated GFP to exhibit subdiffusion in cell nuclei.

A second and closely related point has to do with the molecular origin of anomalous diffusion within regions that contain chromatin. Subdiffusion can result from various types of obstructions or binding interactions. Since unconjugated GFP is not expected to have binding activity, the anomalous behavior observed in chromosomal regions must be due to obstructed diffusion through DNA and other elements of chromatin. The anomalous exponent observed in polytene nuclei (α = 0.79) is less than in HeLa nuclei (α = 0.84), which is consistent with a higher obstacle concentration as might be expected for a relatively dense bundle of chromatin in which the polymers are either stationary or moving on a much slower time scale than the GFP diffusion, resulting in transient pockets of GFP. However, both values are well above the asymptotic percolation cluster limit, which is $\alpha \sim 0.53$ in three dimensions.[8,29]

Finally, the observation that GFP diffuses normally in the interchromatin space and measurement of its anomalous exponent in chromatin will serve as a useful basis for future investigations of proteins that may exhibit binding and other biological activity. For example, if future measurements determine that other proteins diffuse anomalously in the interchromatin space of polytene nuclei, it can be reasonably concluded that this result is due to binding heterogeneity and not crowding. Furthermore, the analysis of FRAP experiments intended to probe the DNA-binding properties of other proteins will require a model that accounts for anomalous diffusion in chromosomal regions, in addition to binding.

■ CONCLUSION

We introduce a new model to interpret quantitative measurements from point FRAP in cellular samples over a wide range of diffusion coefficients. This model takes into account reversible photobleaching to distinguish between fluorophore photophysics and anomalous diffusion. Reversible photobleaching plays a key role in many FRAP experiments, and should therefore be accounted for if accurate quantitative information is to be obtained. We found that anomalous diffusion occurs in most cellular samples expressing unconjugated GFP, with the notable exception of the interchromatin space in polytene samples. The Brownian diffusion observed in these samples was a key result that can be used to interpret future experiments that study binding interactions of biologically active proteins.

■ ASSOCIATED CONTENT

Supporting Information

The supporting text includes a derivation of the FRAP model with photophysics (eq 6), an explanation of intermittent data collection and residual weighting for fitting, 95% confidence intervals for alpha values, and accounting for post bleach electronic noise along with seven figures. This material is available free of charge via the Internet at http://pubs.acs.org.

AUTHOR INFORMATION

Corresponding Author

*E-mail: cfecko@unc.edu. Fax: 919-962-2388. Phone: 919-962-0528.

Author Contributions

The manuscript was written through contributions of all authors. All authors have given approval to the final version of the manuscript.

Notes

The authors declare no competing financial interest.

ACKNOWLEDGMENTS

The authors would like to thank Collin McKinney of the UNC Chemistry Electronics facility and Michael Tycon for their assistance in designing and constructing the point FRAP preamp and Dr. John Papanikolas for allowing the use of his lab's equipment in troubleshooting and designing the preamp. We also thank Dr. Gary Pielak for providing the GFP used in solution experiments and Lori Nichols for writing the LabView software used to control the two-photon microscope. This research was supported by the National Science Foundation under Grant No. PHY-1150017.

ABBREVIATIONS

FRAP, fluorescence recovery after photobleaching; GFP, enhanced green fluorescent protein; FCS, fluorescence correlation spectroscopy; PBS, phosphate buffered saline; PMT, photomultiplier tube; BIC, Bayesian information criterion

REFERENCES

(1) Periasamy, N.; Verkman, A. S. Analysis of Fluorophore Diffusion by Continuous Distributions of Diffusion Coefficients: Application to Photobleaching Measurements of Multicomponent and Anomalous Diffusion. *Biophys. J.* **1998**, *75*, 557−567.

(2) Banks, D. S.; Fradin, C. Anomalous Diffusion of Proteins Due to Molecular Crowding. *Biophys. J.* **2005**, *89*, 2960−2971.

(3) Masuda, A.; Ushida, K.; Okamoto, T. New Fluorescence Correlation Spectroscopy Enabling Direct Observation of Spatiotemporal Dependence of Diffusion Constants as an Evidence of Anomalous Transport in Extracellular Matrices. *Biophys. J.* **2005**, *88*, 3584−3591.

(4) Haugh, J. M. Analysis of Reaction-Diffusion Systems with Anomalous Subdiffusion. *Biophys. J.* **2009**, *97*, 435−442.

(5) Bancaud, A.; Huet, S.; Daigle, N.; Mozziconacci, J.; Beaudouin, J.; Ellenberg, J. Molecular Crowding Affects Diffusion and Binding of Nuclear Proteins in Heterochromatin and Reveals the Fractal Organization of Chromatin. *EMBO J.* **2009**, *28*, 3785−3798.

(6) Wu, J.; Corbett, A. H.; Berland, K. M. The Intracellular Mobility of Nuclear Import Receptors and NLS Cargoes. *Biophys. J.* **2009**, *96*, 3840−3849.

(7) Guigas, G.; Kalla, C.; Weiss, M. The Degree of Macromolecular Crowding in the Cytoplasm and Nucleoplasm of Mammalian Cells is Conserved. *FEBS Lett.* **2007**, *581*, 5094−5098.

(8) Weiss, M.; Elsner, M.; Kartberg, F.; Nilsson, T. Anomalous Subdiffusion Is a Measure for Cytoplasmic Crowding in Living Cells. *Biophys. J.* **2004**, *87*, 3518−3524.

(9) Guigas, G.; Weiss, M. Sampling the Cell with Anomalous Diffusion—The Discovery of Slowness. *Biophys. J.* **2008**, *94*, 90−94.

(10) Sereshki, L. E.; Lomholt, M. A.; Metzler, R. A Solution to the Subdiffusion-efficiency Paradox: Inactive States Enhance Reaction Efficiency at Subdiffusion Conditions in Living Cells. *Europhys. Lett.* **2012**, *97*, 20008.

(11) Saxton, M. J. Anomalous Subdiffusion in Fluorescence Photobleaching Recovery: A Monte Carlo Study. *Biophys. J.* **2001**, *81*, 2226−2240.

(12) Sokolov, I. M. Models of Anomalous Diffusion in Crowded Environments. *Soft Matter* **2012**, *8*, 9043−9052.

(13) Sprague, B. L.; Pego, R. L.; Stavreva, D. A.; McNally, J. G. Analysis of Binding Reactions by Fluorescence Recovery after Photobleaching. *Biophys. J.* **2004**, *86*, 3473−3495.

(14) Kang, M.; Day, C. A.; DiBenedetto, E.; Kenworthy, A. K. A Quantitative Approach to Analyze Binding Diffusion Kinetics by Confocal FRAP. *Biophys. J.* **2010**, *99*, 2737−2747.

(15) Axelrod, D.; Koppel, D. E.; Schlessinger, J.; Elson, E.; Webb, W. W. Mobility Measurement by Analysis of Fluorescence Photobleaching Recovery Kinetics. *Biophys. J.* **1976**, *16*, 1055−1069.

(16) Braga, J.; Desterro, J. M. P.; Carmo-Fonseca, M. Intracellular Macromolecular Mobility Measured by Fluorescence Recovery after Photobleaching with Confocal Laser Scanning Microscopes. *Mol. Biol. Cell* **2004**, *15*, 4749−4760.

(17) Braeckmans, K.; Remaut, K.; Vandenbroucke, R. E.; Lucas, B.; De Smedt, S. C.; Demeester, J. Line FRAP with the Confocal Laser Scanning Microscope for Diffusion Measurements in Small Regions of 3-D Samples. *Biophys. J.* **2007**, *92*, 2172−2183.

(18) Kang, M.; Day, C. A.; Drake, K.; Kenworthy, A. K.; DiBenedetto, E. A Generalization of Theory for Two-Dimensional Fluorescence Recovery after Photobleaching Applicable to Confocal Laser Scanning Microscopes. *Biophys. J.* **2009**, *97*, 1501−1511.

(19) Smisdom, N.; Braeckmans, K.; Deschout, H.; vandeVen, M.; Rigo, J.; De Smedt, S. C.; Ameloot, M. Fluorescence Recovery after Photobleaching on the Confocal Laser-scanning Microscope: Generalized Model without Restriction on the Size of the Photobleached Disk. *J. Biomed. Opt.* **2011**, *16*, 046021−046021.

(20) Mueller, F.; Mazza, D.; Stasevich, T. J.; McNally, J. G. FRAP and Kinetic Modeling in the Analysis of Nuclear Protein Dynamics: What do We Really Know? *Curr. Opin. Cell Biol.* **2010**, *22*, 403−411.

(21) Mueller, F.; Wach, P.; McNally, J. G. Evidence for a Common Mode of Transcription Factor Interaction with Chromatin as Revealed by Improved Quantitative Fluorescence Recovery after Photobleaching. *Biophys. J.* **2008**, *94*, 3323−3339.

(22) Lakowicz, J. R., Ed. *Nonlinear and Two-photon-induced Fluorescence*; Topics in Fluorescence Spectroscopy; Kluwer Academic Publishers: New York, 1997; Vol. 5.

(23) Denk, W.; Strickler, J. H.; Webb, W. W. Two-Photon Laser Scanning Fluorescence Microscopy. *Science* **1990**, *248*, 73−76.

(24) Zipfel, W. R.; Williams, R. M.; Webb, W. W. Nonlinear Magic: Multiphoton Microscopy in the Biosciences. *Nat. Biotechnol.* **2003**, *21*, 1369−1377.

(25) Brown, E. B.; Wu, E. S.; Zipfel, W. R.; Webb, W. W. Measurement of Molecular Diffusion in Solution by Multiphoton Fluorescence Photobleaching Recovery. *Biophys. J.* **1999**, *77*, 2837−2849.

(26) Calvert, P. D.; Peet, J. A.; Bragin, A.; Schiesser, W. E.; Pugh, E. N. Fluorescence Relaxation in 3D from Diffraction-limited Sources of PAGFP or Sinks of EGFP Created by Multiphoton Photoconversion. *J. Microsc.* **2007**, *225*, 49−71.

(27) Schnell, E. A.; Eikenes, L.; Tufto, I.; Erikson, A.; Juthajan, A.; Lindgren, M.; de, L. D. Diffusion Measured by Fluorescence Recovery after Photobleaching based on Multiphoton Excitation Laser Scanning Microscopy. *J. Biomed. Opt.* **2008**, *13*, 064037−064037.

(28) Feder, T. J.; Burst-Mascher, I.; Slattery, J. P.; Baird, B.; Webb, W. W. Constrained Diffusion or Immobile Fraction on Cell Surfaces: A New Interpretation. *Biophys. J.* **1996**, *70*, 2767−2773.

(29) Bouchaud, J.; Georges, A. Anomalous Diffusion in Disordered Media: Statistical Mechanisms, Models and Physical Applications. *Phys. Rep.* **1990**, *195*, 127−293.

(30) Braeckmans, K.; Stubbe, B. G.; Remaut, K.; Demeester, J.; De Smedt, S. C. Anomalous Photobleaching in Fluorescence Recovery after Photobleaching Measurements due to Excitation Saturation a Case Study for Fluorescein. *J. Biomed. Opt.* **2006**, *11*, 044013−044013.

(31) Stasevich, T. J.; Mueller, F.; Michelman-Ribeiro, A.; Rosales, T.; Knutson, J. R.; McNally, J. G. Cross-Validating FRAP and FCS to Quantify the Impact of Photobleaching on In Vivo Binding Estimates. *Biophys. J.* **2010**, *99*, 3093−3101.
(32) Mueller, F.; Morisaki, T.; Mazza, D.; McNally, J. Minimizing the Impact of Photoswitching of Fluorescent Proteins on FRAP Analysis. *Biophys. J.* **2012**, *102*, 1656−1665.
(33) Hoyt, L. F. New Table of the Refractive Index of Pure Glycerol at 20°C. *Ind. Eng. Chem.* **1934**, *26*, 329−332.
(34) Zobeck, K. L.; Buckley, M. S.; Zipfel, W. R.; Lis, J. T. Recruitment Timing and Dynamics of Transcription Factors at the Hsp70 Loci in Living Cells. *Mol. Cell* **2010**, *40*, 965−975.
(35) Daddysman, M.; Fecko, C. DNA Multiphoton Absorption Generates Localized Damage for Studying Repair Dynamics in Live Cells. *Biophys. J.* **2011**, *101*, 2294−2303.
(36) Schwarz, G. Estimating The Dimension of a Model. *Ann. Stat.* **1978**, *6*, 461−464.
(37) Akaike, H. A New Look at the Bayes Procedure. *Biometrika* **1978**, *65*, 53−59.
(38) Claeskens, G.; Hjort, N. L. *Model Selection and Model Averaging*; Cambridge University Press: Cambridge, U.K., 2008.
(39) Kang, M.; DiBenedetto, E.; Kenworthy, A. Proposed Correction to Feder's Anomalous Diffusion FRAP Equations. *Biophys. J.* **2011**, *100*, 791−792.
(40) Dickson, R. M.; Cubitt, A. B.; Tsien, R. Y.; Moerner, W. E. On/off Blinking and Switching Behaviour of Single Molecules of Green Fluorescent Protein. *Nature* **1997**, *388*, 355−358.
(41) Sinnecker, D.; Voigt, P.; Hellwig, N.; Schaefer, M. Reversible Photobleaching of Enhanced Green Fluorescent Proteins. *Biochemistry* **2005**, *44*, 7085−7094.
(42) Petrášek, Z.; Schwille, P. Precise Measurement of Diffusion Coefficients using Scanning Fluorescence Correlation Spectroscopy. *Biophys. J.* **2008**, *94*, 1437−1448.
(43) Miller, G. G.; Raleigh, J. A. Action of Some Hydroxyl Radical Scavengers on Radiation-Induced Haemolysis. *Int. J. Radiat. Biol.* **1983**, *43*, 411−419.
(44) Segur, J. B.; Oberstar, H. E. Viscosity of Glycerol and Its Aqueous Solutions. *Ind. Eng. Chem.* **1951**, *43*, 2117−2120.
(45) Chattopadhyay, K.; Saffarian, S.; Elson, E. L.; Frieden, C. Measuring Unfolding of Proteins in the Presence of Denaturant Using Fluorescence Correlation Spectroscopy. *Biophys. J.* **2005**, *88*, 1413−1422.